EFFECT OF THE CORRECTED IONIZATION POTENTIAL AND SPATIAL DISTRIBUTION ON THE ANGULAR AND ENERGY DISTRIBUTION IN TUNNEL IONIZATION

V. M. Petrović, T. B. Miladinović[*]

Department of Physics, Faculty of Science, Kragujevac University
34000, Kragujevac, Serbia

Within the framework of the Ammosov–Delone–Krainov theory, we consider the angular and energy distribution of outgoing electrons due to ionization by a circularly polarized electromagnetic field. A correction of the ground ionization potential by the ponderomotive and Stark shift is incorporated in both distributions. Spatial dependence is analyzed.

1. INTRODUCTION

Tunnel ionization of atoms is an important mechanism of laser ionization. There are several theoretical approaches to the calculation of the tunnel ionization rate. The oldest is Keldysh's approach [1] based on the assumption known as the strong-field approximation [2]. In [1], Keldysh introduced the well-known parameter $\gamma = \sqrt{E_i/2U_p}$ (E_i is the unperturbed ionization energy and U_p is the ponderomotive potential) that determines whether the photoionization process lies in the tunneling or multiphoton region. For $\gamma \ll 1$, the tunnel ionization is a dominant ionization process. Soon after this work, Perelomov, Popov, and Terent'ev developed the PPT model [3]. Finally, Ammosov, Delone, and Krainov extended the PPT theory and derived the ADK theory, which we use here [4]. Within the framework of the ADK theory, the ionization rate for a circularly polarized laser field is [5]

$$W_{cir}^{ADK} = \frac{F_{cir} D_{cir}^2}{8\pi Z} \exp\left(-\frac{Z}{3n^{*3}F_{cir}E_i}\right),$$

where

$$D_{cir} \equiv \left(\frac{4Z^3 e}{F_{cir} n^{*4}}\right)^{n^*}, \quad F_{cir} = \frac{19\sqrt{I}}{5.1 \cdot 10^9},$$

I is the laser field intensity, and $n^* = Z/\sqrt{2E_i}$ is the effective principal quantum number (Z is the ion charge).

The purpose of this paper is to improve the angular and energy distributions of ejected photoelectrons with the corrections of the unperturbed ionization potential caused by laser irradiation taken into account.

2. THEORETICAL FRAMEWORK

In particular cases of circular polarizations of the ionizing field, the angular distribution of photoelectrons emerging from tunnel ionization is described by [5]

$$W(\theta) = W(0) \exp\left(-\frac{F_{cir}\sqrt{2E_i}}{\omega^2}\theta^2\right), \qquad (1)$$

where θ is the azimuthal angle and $W(0) = W_{cir}^{ADK}$ is the tunneling rate. The nonzero initial electron influences the tunneling rate, and we therefore use the modified expression [6]

$$W_{cir,p}^{ADK} = \frac{F_{cir} D_{cir}^2}{8\pi Z} \exp\left(-\frac{Z}{3n^{*3}F_{cir}E_i} - \frac{p^2\gamma^3}{3\omega}\right).$$

Just after leaving the barrier, the momentum of the ejected photoelectron is p. Because the ionization probabilities in static and alternating electric fields are different only by a preexponential factor [3], it is convenient to use the parabolic coordinate to express the initial momentum outside the barrier as

$$p = \frac{1}{2}\left(\sqrt{F_{cir}\eta - 1} - \frac{1}{\eta\sqrt{F_{cir}\eta - 1}}\right),$$

---
[*] E-mail: tanja.miladinovic@gmail.com

where η is the parabolic coordinate, $\eta > 1/F_{cir}$ [7]. If the system total energy is independent of the coordinate η, the momentum is conserved along the classical path, i. e., $p_\eta = p$ [8].

The corresponding spectrum width is defined as

$$\Delta\theta = \frac{\omega}{\sqrt[4]{2E_i F_{cir}^2}} . \qquad (2)$$

Another variable of interest is the energy distribution of the ejected photoelectrons [9],

$$W(E) = W_{max} \exp\left[-\frac{\gamma^3}{2E_i\omega}\left(E - \frac{F_{cir}^2}{2\omega^2}\right)^2\right], \qquad (3)$$

where W_{max} is the maximal value of the ionization rate determined by the relation [5]

$$W_{max} = \frac{\omega^2 D_{cir}^2}{8\sqrt{\pi^3 n^* Z F_{cir}}} \times$$
$$\times \exp\left[-\frac{2(2E_i)^{3/2}}{3F_{cir}}\left(1 - \frac{\gamma^2}{15}\right)\right]. \qquad (4)$$

Substituting $E = p^2/2$ in Eq. (3), we obtain

$$W(E) = W_{max} \exp\left[-\frac{\gamma^3}{2E_i\omega}\left(\frac{p^2}{2} - \frac{F_{cir}^2}{2\omega^2}\right)^2\right]. \qquad (5)$$

Both the angular and the energy spectra of the ejected photoelectrons depend on the ionization potential. As it is changed by the laser field, these changes should be incorporated into Eqs. (1) and (5). We consider two effects, the ponderomotive shift and the linear Stark shift.

The ponderomotive potential is related with the wiggle motion of the ejected photoelectrons in response to an applied laser field of strength F and frequency ω. Assuming velocities of the ejected photoelectrons $\nu_e \ll c$ (where c is speed of light), we have the ponderomotive potential for circular polarization $U_p = F_{cir}^2/2\omega^2$, which is the cycle-average kinetic energy of an electron oscillating in the applied laser field. An oscillating electric field of the laser also induces an intensity-dependent shift of the atomic levels, called the Stark shift. For our purpose, we take these corrections into account and obtain the effective ionization potential

$$E_i^{eff} = E_i + U_p + E_{st} = E_i + \frac{F_{cir}^2}{2\omega^2} + \frac{\alpha F_{cir}^2}{4},$$

where α is the static polarizability of the atom [10].

The Gaussian spatial intensity distribution can be expressed as a function of the axial coordinate ρ [11]:

$$F(\rho) = F \exp\left[-2\left(\frac{\rho}{R}\right)^2\right], \qquad (6)$$

where

$$\rho = R\sqrt{1 + \left(\frac{\lambda\eta}{\pi R^2}\right)^2}$$

is the axial coordinate that is normal to the light ray [12] and R is the radius of the laser beam.

After inserting Eq. (6) into Eqs. (1) and (5), we obtain the angular distribution

$$W_G(\theta) = W(0) \times$$
$$\times \exp\left[-\frac{F_{cir}\exp\left[-2\left(\frac{\rho}{R}\right)^2\right]\sqrt{2E_i}}{\omega^2}\theta^2\right] \qquad (7)$$

and the energy distribution

$$W_G(E) = W_{max} \times$$
$$\times \exp\left[-\frac{\gamma^3}{2E_i\omega}\left(\frac{p^2}{2} - \frac{F_{cir}\exp\left[-2\left(\frac{\rho}{R}\right)^2\right]^2}{2\omega^2}\right)^2\right]. \qquad (8)$$

3. ANALYSIS

We investigated the angular and energy spectra of the ejected photoelectrons for the tunneling regime, $\gamma = 0.3 \ll 1$, induced by a circularly polarized laser field whose intensity varied between 10^{14} W·cm^{-2} and 10^{16} W·cm^{-2}. We observed the argon atom, Ar, with $Z = 1$. We assumed that the electron velocity is small compared to the speed of light and applied a nonrelativistic calculation. In this case, besides the general case, we use the Gaussian laser pulse with the wavelength $\lambda = 800$ nm. It can be easily seen that the photon energy $\omega = 0.05696$ is small compared to the ionization potential of the observed atom, which is the condition for the strong-field approximation. The atomic system of units is used, with $e = m_e = \hbar = 1$.

We start from the angular spectra (see Eqs. (1) and (7)). The obtained theoretical curves are shown in Fig. 1. The following notation is used: a variable without a subscript is a value without any correction, the subscript "p" denotes the momentum, "Up" means the ponderomotive potential, and "St" denotes the Stark shift included.

As can be seen from Eq. (1), the probability angular distribution is dependent on the scattering angle, and the dependence is described by an exponential decreasing as the scattering angle increases. In the intensity range under consideration, the scattering angle ranges within $-0.5 < \theta < 0.5$ for the fixed parabolic coordinate $\eta = 100$. Also, we see that the angular distribution clearly depends on the ionization potential. This
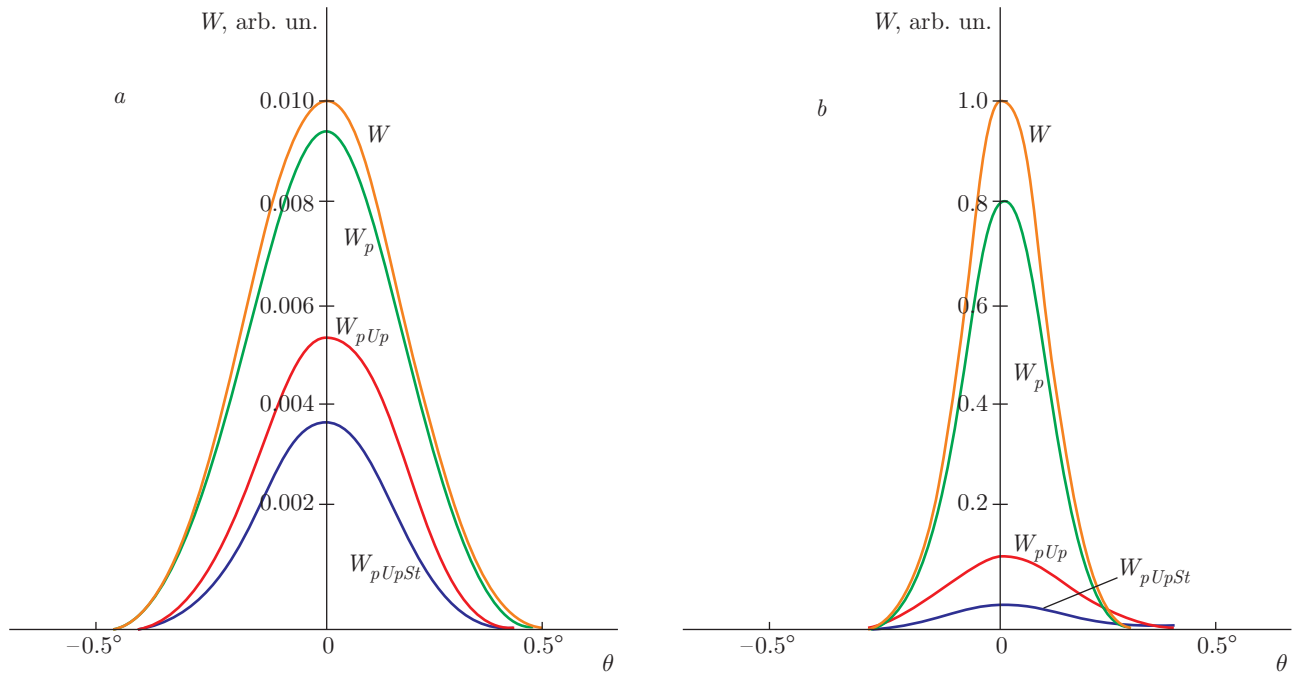
Fig. 1. The angular spectra $W(\theta)$ for a fixed value of the field intensity a) $I = 10^{14}$ W·cm^{-2} and b) $I = 10^{15}$ W·cm^{-2}

is due to the fact that under the condition of the same scattering angle and the same laser intensity, the maximal value of the distribution is significantly reduced. It follows that the ground-state shift caused by the ponderomotive and the Stark shift cannot be neglected in the analysis. It is obvious from Fig. 1 that increasing the laser field intensity results in a much lower maximal value of the angular distribution as well as in a sharper range of the angular distribution of photoelectrons. With an increase in the laser intensity, the ponderomotive potential becomes larger, as does the Stark shift. For $= 10^{15}$ W·cm^{-2}, up to the scattering angle $\theta \approx 0.3$, $W(\theta)$ approaches zero. It is clear that in both cases, the angular distribution is concentrated in the region of small scattering angles.

Figure 2 demonstrates the laser intensity dependence of $W(\theta)$ for different scattering angles θ.

In accordance with Fig. 1, with increasing the scattering angle, the angular distribution decreases.

The 3D plot in Fig. 3 demonstrates the angular distribution as a function of the laser field intensity and the scattering angle.

Next, we considered the influence of the spatial beam shape on the angular distribution. Lasers usually emit beams with a Gaussian profile. The influence of the chosen laser profile is accomplished by calculating the angular spectra for the general assumed beam shape as well as the Gaussian shape. The result is
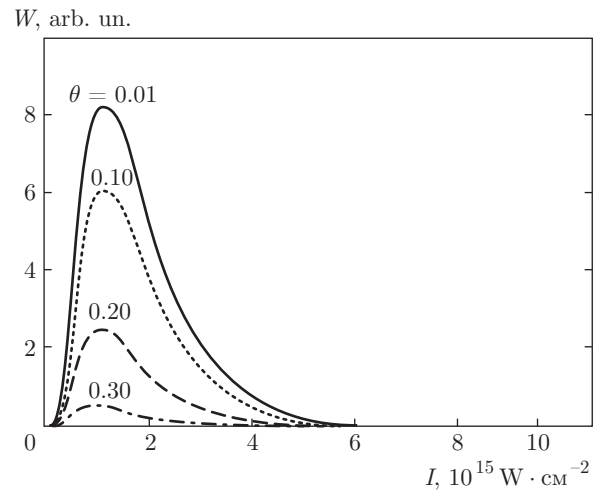

Fig. 2. The angular distribution spectra $W(\theta)$ versus the laser field intensity for different fixed values of the scattering angle θ. The parabolic coordinate is fixed at $\eta = 100$

presented in Fig. 4, which shows that the spatial distribution of the laser intensity influences the angular spectra. The maximal obtained value is reduced. The behavior of the theoretical curves stays mostly the same in both observed cases.

Next, in Fig. 5, we plot the angular distribution width based on Eq. (2). Increasing the laser field in-
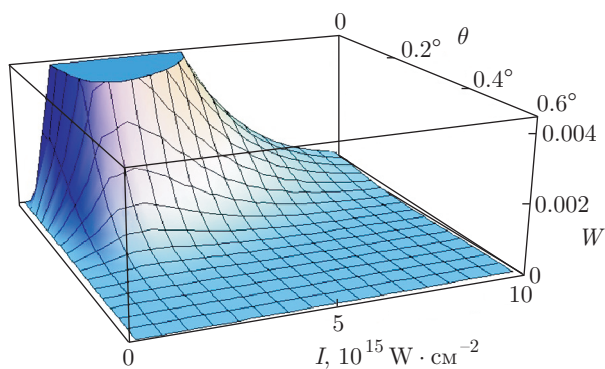
946

Fig. 3. 3D plot of the angular distribution for the fixed value of the parabolic coordinate at $\eta = 100$; the scattering angle varied in range $0 < \theta < 0.6$ and the laser field intensity $10^{14} < I < 10^{16}$ W·cm^{-2}

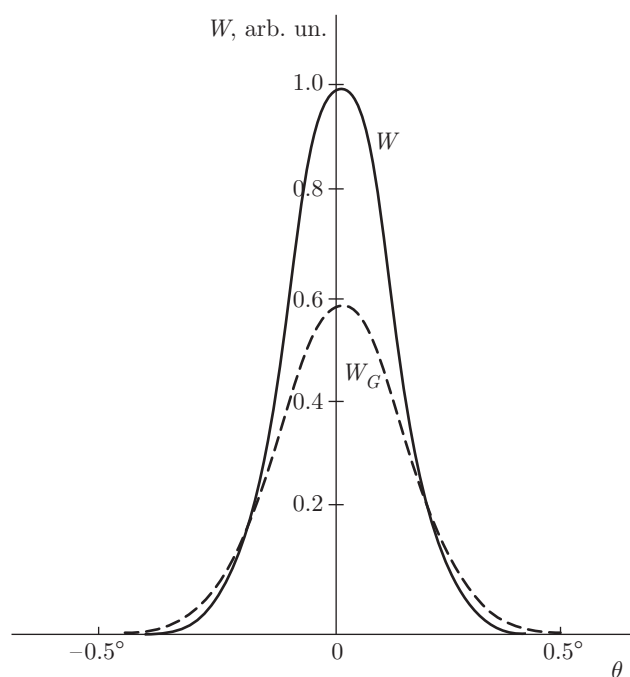**Fig. 4.** The angular spectra as a function of the scattering angle for the fixed field intensity $I = 10^{15}$ W·cm^{-2}

tensity decreases the angular distribution width, first rapidly and then more slowly. This is in accordance with the conclusion about the laser field influence (see Fig. 1).

Similarly to the above, we examin the dependence of the energy distribution of the ejected photoelectrons on the laser field intensity. For this purpose, we plot the corresponding theoretical curves (see Eq. (5)) in Fig. 6.

According to Fig. 6a, including the corrected ionization energy in the formula for the energy distribution reduces the maximal energy distribution value
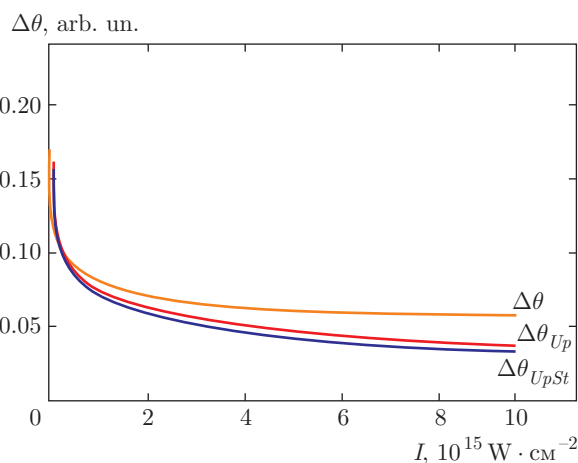

Fig. 5. The angular distribution width versus the laser field intensity

and moves the maximum to a lower field intensity. The energy distribution of an Ar atom has also been analyzed at different parabolic coordinates and laser field intensities. As a result, a 3D plot is obtained (Fig. 6b). Increasing the field intensity enhances the energy distribution, plot first rapidly and then more slowly.

Finally, it is of interest to examine the spatial dependence of the energy distribution. If we specify a particular value of the parabolic coordinate η, the following curves are obtained based on Eq. (8).

Applying the Gaussian beam shape moves the energy distribution curve to higher field intensities. We therefore separate the obtained curves into two graphs. Also, we cut off the increasing part of curves to show that the Gaussian gives monotonously increasing curves. For higher values of the laser field intensity, both curves acquire the characteristic flow shown in Fig. 6a.

4. CONCLUSION

The used ADK theory does not take the ponderomotive shift and the Stark shift into account. Replacing the field free ionization potential with the corrected one, we analyzed how these effects affect the angular and energy distributions. The analysis of the obtained theoretical curves shows that these effects must be taken into account no matter how small they are. Also, the laser beam shape influences the behavior of the considered distribution.
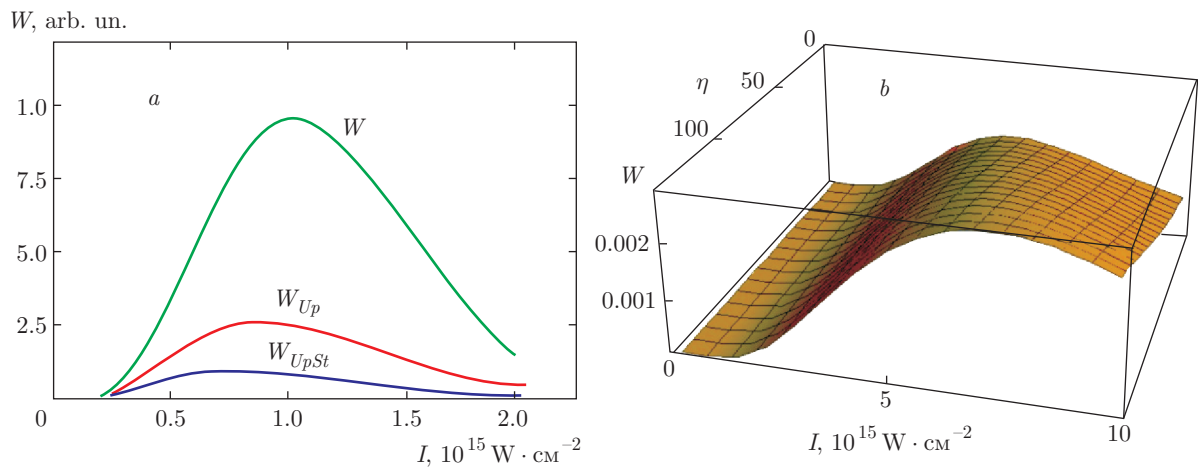
3*

Fig. 6. Theoretical energy spectra versus the laser field intensity: *a*) 2D plot, for the fixed value of the parabolic coordinate $\eta = 140$ and the range of the laser field intensity $10^{15} < I < 2 \cdot 10^{15}$ W·cm^{-2}, *b*) 3D plot, the parabolic coordinate varies in a range $10 < \theta < 140$ and the laser field intensity $10^{14} < I < 10^{15}$ W·cm^{-2}
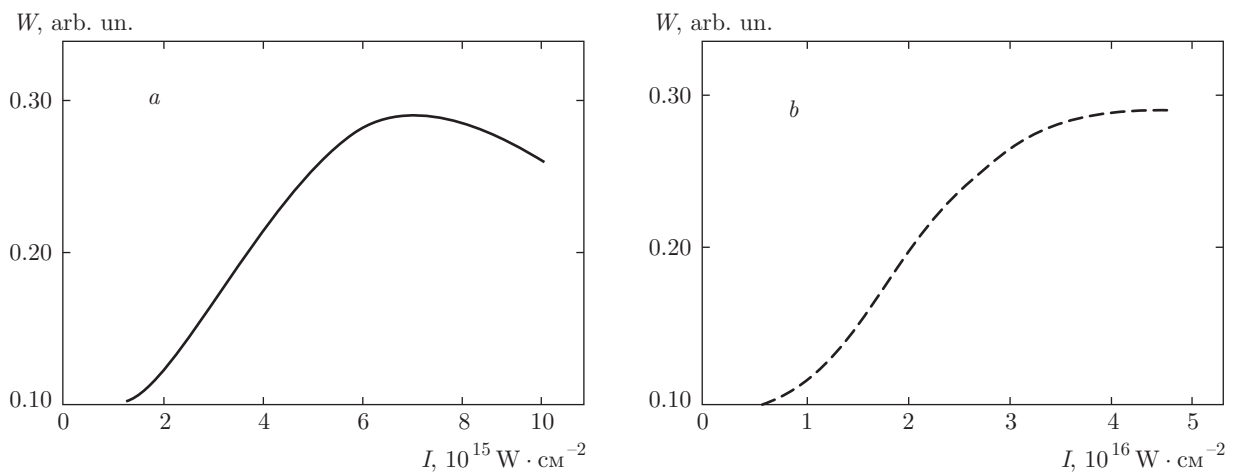

Fig. 7. The energy spectra: *a*) general case, *b*) Gaussian beam profile

REFERENCES

1. L. V. Keldysh, Sov. Phys. JETP **21**, 1135 (1965).

2. J. H. Bauer, Acta Phys. Polon. A **114**, 739 (2008).

3. A. M. Perelomov, V. S. Popov, and M. V. Terent'ev, Sov. Phys. JETR **23**, 924 (1966).

4. V. M. Ammosov, N. B. Delone, and V. P. Krainov, Sov. Phys. JETP **64**, 1191 (1986).

5. N. B. Delone and V. P. Krainov, Phys. Usp. **41**, 469 (1998).

6. V. M. Ristić, T. B. Miladinović, and M. M. Radulović, Acta Phys. Polon. A **112**, 909 (2007).

7. D. Bauer, *Theory of Intense Laser-Matter Interaction*, Max Planck Institute, Heidelberg, Germany (2006).

8. L. D. Landau and E. M. Lifshitz, *Course of Theoretical Physics*: *Volume* 3. *Quantum Mechanics*: *Non Relativistic Theory*, Nauka, Moscow (1989); Pergamon, Oxford (1991).

9. N. B. Delone, I. Yu. Kiyan, and V. P. Krainov, Laser Phys. **3**, 312 (1993).

10. http://ctcp.massey.ac.nz/Tablepol-2.11.pdf.

11. V. M. Petrović and T. B. Miladinović, JETP **4**, 741 (2014).

12. http://www.colorado.edu/physics/phys3340/phys3340 _sp12/CourseInformation/Optics/Gaussian%20Beams %20Lab%20Guide.pdf.